

SERA-H: Beyond Native Sentinel Spatial Limits for High-Resolution Canopy Height Mapping

Thomas Boudras^a, Martin Schwartz^a, Rasmus Fensholt^d, Martin Brandt^d, Ibrahim Fayad^{a,b}, Jean-Pierre Wigneron^e, Gabriel Belouze^{a,f}, Fajwel Fogel^c, Philippe Ciais^a

^a*Laboratoire des Sciences du Climat et de l'Environnement (LSCE), CEA, CNRS, UVSQ, Université Paris-Saclay, Gif-sur-Yvette, France*
^b*Kayros SAS, Paris, 75009, France*

^c*CNRS & Département d'Informatique, École Normale Supérieure – PSL, 45 Rue d'Ulm, 75005, Paris, France*

^d*Department of Geography and Geology, University of Copenhagen, Øster Voldgade 10, Copenhagen, DK-1350, Denmark*

^e*INRAE, Bordeaux Aquitaine Center, 71 avenue E. Bourlaux, CS 20032, 33882, Villenave d'Ornon, France*

^f*Department of Information Systems, University of Münster, Münster, Germany*

Abstract

High-resolution mapping of canopy height is essential for forest management and biodiversity monitoring. Although recent studies have led to the advent of deep learning methods using satellite imagery to predict height maps, these approaches often face a trade-off between data accessibility and spatial resolution. To overcome these limitations, we present SERA-H, an end-to-end model combining a super-resolution module (EDSR) and temporal attention encoding (UTAE). Trained under the supervision of high-density LiDAR data (ALS), our model generates 2.5 m resolution height maps from freely available Sentinel-1 and Sentinel-2 (10 m) time series data. Evaluated on an open-source benchmark dataset in France, SERA-H, with a MAE of 2.6 m and R^2 of 0.82, not only outperforms standard Sentinel-1/2 baselines but also achieves performance comparable to or better than methods relying on commercial very high-resolution imagery (SPOT-6/7, PlanetScope, Maxar). These results demonstrate that combining high-resolution supervision with the spatiotemporal information embedded in time series enables the reconstruction of details beyond the input sensors' native resolution. SERA-H opens the possibility of freely mapping forests with high revisit frequency, achieving accuracy comparable to that of costly commercial imagery.

Keywords:

Deep Learning, Forest Height, Time Series, Sentinel, ALS, Super-Resolution, Attention Encoder

1. Introduction

Accurate canopy height mapping is essential for understanding forest ecosystems, estimating biomass and stored carbon, and monitoring forest dynamics (Lefsky et al., 2002; Goetz et al., 2010; Schwartz et al., 2023; Tomppo, 2008; Bossy et al., 2025). Such maps are valuable for sustainable forest management, biodiversity assessment, and climate change mitigation policies.

Canopy height maps can be derived by processing data from Airborne Laser Scanning (ALS) and NASA's Global Ecosystem Dynamics Investigation (GEDI). Direct measurements are also obtained from National Forest Inventories (NFIs) at point locations. While the GEDI mission has established itself as the reference for monitoring the vertical structure of forests on a global scale, it operates by nature as a sampling mission providing sparse spatial and temporal samples (so-called

footprints). ALS is the reference for high-resolution local canopy height mapping, but its deployment remains costly and geographically limited. As for NFI inventories, although they provide direct *in-situ* measurements, they remain limited to a small number of plot locations and do not allow for continuous spatial monitoring. To overcome the discontinuity of these reference measurements, deep learning approaches have emerged as an effective solution. These approaches exploit the continuous spatial and temporal coverage of optical (e.g., Sentinel-2, Landsat, SPOT) and radar (e.g., Sentinel-1, PALSAR-2) imagery to predict canopy height maps under the supervision of LiDAR acquisitions, such as those from GEDI or ALS data. This enables large-scale canopy height prediction using data that is both frequently updated and cost-effective.

Recently, several deep learning approaches have pro-

duced canopy height maps derived from open-access satellite data (Lang et al., 2023; Schwartz et al., 2025; Pauls et al., 2025). However, the level of detail in these maps remains constrained by the spatial resolution of the source imagery (at best 10 m resolution with Sentinel-2). Therefore, these maps can at best go as far as the tree group level, but never into greater detail. To overcome these spatial limitations and to achieve the precision closest to the individual tree level, recent approaches have focused on using very high-resolution commercial imagery (e.g., Maxar (Tolan et al., 2024), PlanetScope (Liu et al., 2023), SPOT-6/7 (Fogel et al., 2025)). However, while these imagery sources offer superior spatial detail, they suffer from either restricted access, limited spatial coverage, or high costs.

Recently, open access to ALS data has expanded significantly (LiDAR HD program¹, Fischer et al. (2025)) providing extensive coverage of high-quality data. Beyond serving as the most accurate reference for locally estimating canopy height (Alexander et al., 2018; Lefsky et al., 2005), ALS datasets offer a very high spatial resolution (typically 1-2 m). On the other hand, the highest resolution provided by open-access satellite data comes from the Sentinel missions, part of ESA's Copernicus Earth Observation program. At 10 m, the resolution of Sentinel-1 and Sentinel-2 satellite images remains considerably coarser than the level of detail offered by ALS-based canopy height maps. To match the resolution of the input imagery with the reference data for model training, the most common approach is to downgrade the resolution of the canopy height derived from ALS data to align it with the Sentinel resolution (Liu et al., 2023; Su et al., 2025b,a), inevitably resulting in significant information loss. Here, we propose an alternative approach: to increase the resolution of Sentinel images to match the fidelity of ALS-derived canopy height maps.

To increase the spatial resolution of images, a solution is the application of super-resolution, a method for reconstructing high-resolution images from lower-resolution data. Super-resolution techniques are widely applied in urban remote sensing: Several building segmentation models employ a two-step sequential pipeline, in which a super-resolution deep learning model first upsamples the image, serving as a pre-processing step for a separate model dedicated to building detection (Chen et al., 2023; Zhang et al., 2021). End-to-end architectures have also been implemented, integrating super-resolution and segmentation within a unified

network in order to simultaneously optimize both tasks (Ayala et al., 2022).

At the same time, a recent study has demonstrated the value of directly exploiting the time series of raw Sentinel-2 images, in contrast to the standard practice of using annual or seasonal mosaics, to estimate canopy height (Pauls et al., 2025). By avoiding the loss of information inherent in annual compositing, this model exploits the seasonal and intra-annual dynamics of input Sentinel-2 images, significantly improving the accuracy of height predictions, particularly for tall trees. Another study by Sirko et al. (2023) combined a super-resolution approach and multi-temporal images, by simultaneously using spatial and temporal variations in successive acquisitions to produce higher-resolution results in various urban remote sensing contexts. Their model has proven effective for tasks such as building segmentation, centroid and height estimation, and road segmentation. Fundamentally, this performance relies on exploiting the sub-pixel shifts inherent in revisited acquisitions, which allows the model to resolve aliasing and reconstruct fine spatial details by leveraging this temporal redundancy. However, to our knowledge, no study combining super-resolution and multi-temporal images for forestry applications exists to date.

Current methods lack the capacity to generate canopy height maps at a near-individual tree scale without relying on costly, restricted, or infrequent commercial imagery. To address this limitation, we introduce SERA-H (Super-resolution for Environmental Rapid Analysis - Height), an end-to-end deep learning framework designed to generate very high-resolution (2.5 m) canopy height maps directly from coarser Sentinel-1 and Sentinel-2 time series (10 m). Our approach aims to fully leverage the input data to surpass their native resolution, thereby avoiding the information loss typically induced by downsampling ALS reference data. To achieve this, we combine a super-resolution module with a temporal attention mechanism designed to process satellite image time series. This article first details the proposed architecture (Section 2). We then present an ablation study to validate our design choices (Section 3.1), before benchmarking our results against recent state-of-the-art methods (Section 3.2).

2. Materials and Methods

2.1. Data

The proposed approach aims to transform Sentinel-1 and Sentinel-2 time series (10 m) into high-resolution canopy height maps (2.5 m) using super-resolution and

¹<https://geoservices.ign.fr/lidarhd>

temporal regression. This section details the datasets used for training and evaluation. We first describe the Open-Canopy benchmark (Section 2.2), which provides the ALS-based reference height maps, the dataset splits, and the vegetation mask. Then, we present the acquisition and processing of the input Sentinel satellite time series (Section 2.2.1).

2.2. Open-Canopy Dataset: Reference Data, Splits, and Vegetation Mask

To train and evaluate our model, we used the Open-Canopy dataset (Fogel et al., 2025), a public benchmark specifically designed for high-resolution canopy height estimation. Derived from the French LiDAR HD campaigns acquired between 2021 and 2023², the Open-Canopy dataset provides ALS-based canopy height maps at 1.5 m resolution which served as reference for height prediction. For the purpose of our study, we downsampled these reference images to 2.5 m using max-pooling aggregation.

The dataset spans 87,383 patches of 1×1 km distributed across France, ensuring a wide diversity of forest types and topographies. We adhered to the fixed spatial partition defined by the Open-Canopy benchmark: 66,339 km² for training, 7,369 km² for validation, and 13,675 km² for testing (Fig. 1), with a 1 km buffer systematically applied around test areas to prevent spatial leakage.

Finally, to ensure that performance metrics focused on relevant areas, we restricted the evaluation to vegetation-covered zones using the vegetation mask provided by the Open-Canopy dataset. This mask was constructed by the union of a LiDAR-derived mask (height > 1.5 m) and IGN forest polygons³. Note that this mask was exclusively applied during the validation and test phases for metric calculation and was not used during training.

2.2.1. Satellite Data: Sentinel-1 and Sentinel-2

Unlike the Open-Canopy benchmark which relied on commercial SPOT-6/7 imagery, our model deployed input imagery from the Sentinel-1 and Sentinel-2 sensor systems, key components of the European Space Agency’s (ESA) Copernicus Earth observation program. These satellite systems provide complementary radar and optical data with global coverage and high temporal resolution. We retrieved these images using the `geefetch` package⁴ (Belouze et al., 2025), which interfaces with the Google Earth Engine (GEE) API⁵. For

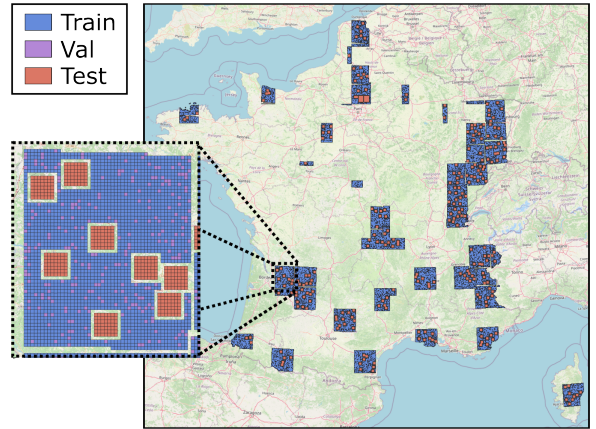


Figure 1: Spatial splits from the Open-Canopy dataset. The inset zooms into a representative region to show the spatial arrangement of the different training, test, and validation tiles. A 1 km buffer zone is applied around the test areas to avoid any spatial leakage.

each patch of the Open-Canopy Dataset, all Sentinel images available within a 120-day window centered on the acquisition date of the corresponding ALS data were retrieved. To minimize the influence of atmospheric perturbations, Sentinel-2 data were subjected to a cloud-masking procedure. Images with more than 40% cloudy pixels or 20% high-probability cloud coverage were excluded. Individual pixels with a cloud probability above 40% or flagged in Sentinel-2’s QA60 band were masked.

For each raw Sentinel-2 ($S2$) image, the closest raw Sentinel-1 ascending ($S1_{asc}$) and descending ($S1_{desc}$) images in time were associated to form a triplet ($S2, S1_{asc}, S1_{desc}$). Ascending and descending acquisitions were distinguished because they have opposite observation angles, offering two complementary viewpoints. Furthermore, combining Sentinel-2 optical images and Sentinel-1 radar images allowed simultaneous exploitation of the spectral and structural properties of the canopy. Across the dataset, we obtained an average of 13.51 triplets per patch.

For Sentinel-2, we selected 10 spectral bands that are relevant for vegetation characterization: the visible RGB channels (B2, B3, B4), the vegetation red-edge bands (B5, B6, B7), the near-infrared (NIR) bands (B8, B8A), and the short-wave infrared (SWIR) bands (B11, B12). Each Sentinel-1 image contained 2 bands for VV and VH polarizations for both ascending and descending orbits. Consequently, each input triplet comprised a total of 14 channels (10 optical and 4 radar), all harmonized at a resolution of 10 m using nearest-neighbor resampling.

²<https://geoservices.ign.fr/lidarhd>

³<https://geoservices.ign.fr/bdforet>

⁴<https://geefetch.readthedocs.io/en/latest/>

⁵<https://earthengine.google.com/>

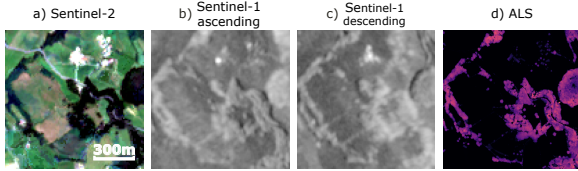


Figure 2: Examples of input and reference data used in SERA-H. (a) Sentinel-2 optical image, (b) Sentinel-1 ascending radar image, and (c) Sentinel-1 descending radar image together form one of the triplet of the time series used as model input. (d) The corresponding ALS-derived canopy height map, resampled at 2.5 m, serves as reference.

2.3. Model

The SERA-H architecture is composed of two primary modules: a super-resolution module (EDSR, Section 2.3.1) and a regression module (UTAE, Section 2.3.2). In the following subsections, we first detail the characteristics of each component individually, and then describe the global end-to-end workflow of the model (Section 2.3.3). We present the full workflow in Fig. 3.

2.3.1. Enhanced Deep Super-resolution (EDSR) Module

Super-resolution reconstructs a high-resolution image from low-resolution inputs by recovering missing details to improve spatial clarity and pixel density. In the field of super-resolution models, Generative Adversarial Networks (GANs) are widely used (Ledig et al., 2016; Jiang et al., 2019; Guo et al., 2022). These models are based on competition between a generator, which synthesizes plausible high-resolution images, and a discriminator responsible for distinguishing between real and generated images. Although this competitive training promotes high visual realism, it encourages the generator to prioritize perceptual plausibility at the expense of strict fidelity to reality, often resulting in the appearance of unwanted artifacts (so-called hallucinations). Consequently, for our task, adversarial approaches were excluded.

Instead, we opted for the Enhanced Deep Super-Resolution (EDSR) model (Lim et al., 2017), which has demonstrated state-of-the-art performance in up-sampling satellite imagery while being less prone to artifacts (Karwowska and Wierzbicki, 2022; Ren et al., 2023). Derived from the ResNet architecture, EDSR optimizes the model by removing unnecessary normalization layers. This simplification allows for a much larger and more powerful network to be built. We thus adopted this architecture in our workflow to upsample each individual image within the time series, increasing the spatial resolution by a factor of 4.

2.3.2. Regression Module: U-Net with Temporal Attention Encoder (UTAE)

For the regression module, we selected the UTAE (U-Net with Temporal Attention Encoder) (Garnot and Lan-drieu, 2022) for its ability to process a complete time series as input and generate a single prediction output. This architecture combines a standard U-Net backbone (Ronneberger et al., 2015) for spatial analysis with a dedicated temporal attention mechanism. Specifically, each image in the series is first encoded independently by the same convolutional encoder. Then, this temporal sequence is fused using a temporal attention mechanism that computed relevance masks to collapse the time dimension into a single representative embedding. This fused representation is finally decoded to reconstruct the high-resolution canopy height map.

2.3.3. Overall Architecture

Our approach relied on the synergy between super-resolution and multi-temporal regression to produce canopy height maps with a spatial resolution finer than that of the native Sentinel imagery. By exploiting the sub-pixel shifts inherent in revisited acquisitions, the model aimed to reconstruct forest structural details at a higher resolution. To achieve this, we implemented an end-to-end architecture, enabling the simultaneous optimization of both the super-resolution (EDSR) and multi-temporal regression (UTAE) modules. By integrating these tasks into a single optimization step, we overcame the limitations of sequential two-stage pipelines, ensuring that the upsampling process was driven by the final canopy height prediction rather than by an intermediate reconstruction metric. The complete model contains 44.2 million trainable parameters, predominantly allocated to the EDSR module (97.5%) compared to the UTAE module (2.5%). The pipeline is illustrated in Fig. 3 and described in detail below.

Input Representation. The input data is formatted into a tensor $e \in \mathbb{R}^{B \times T \times C \times H \times W}$, where B represents the batch size, T the fixed sequence length of the time series, C the number of channels, and (H, W) the spatial dimensions. In our experiments, the shape was $2 \times 16 \times 14 \times 64 \times 64$.

Super-Resolution Module (EDSR). First, the images in the temporal sequence are independently upsampled. To do so, the batch and temporal dimensions are collapsed to form a flattened tensor $e^f \in \mathbb{R}^{(B \cdot T) \times C \times H \times W}$. This tensor is input into the EDSR model, which performs a $4 \times$ spatial upsampling, resulting in the super-

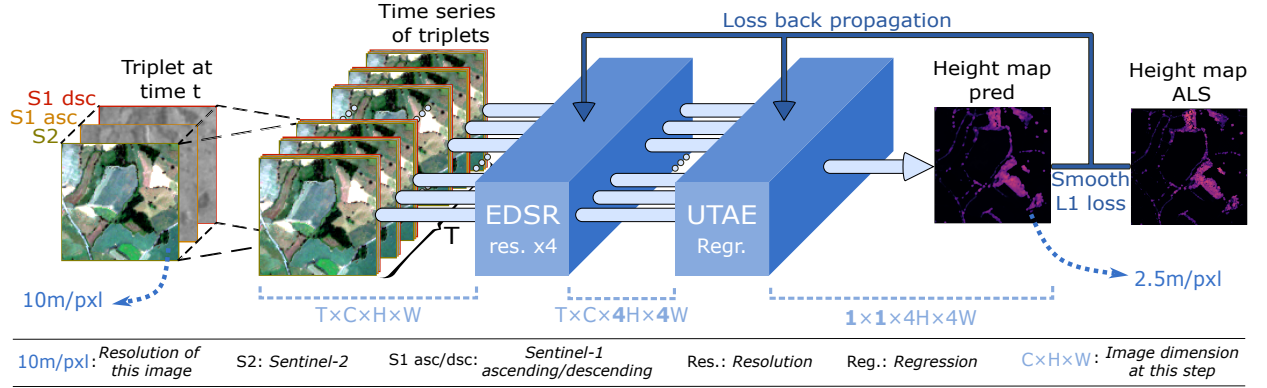


Figure 3: Overview of the SERA-H model workflow. Each input sample consists of a temporal sequence of triplets, where each triplet is composed of one Sentinel-2 optical image and its temporally closest Sentinel-1 ascending and descending acquisitions ($S2, S1_{asc}, S1_{dsc}$). This yields an input tensor of size $T \times C \times H \times W$, where T is the fixed number of triplets in the temporal sequence, C the total number of spectral and radar channels per triplet, and H and W the spatial dimensions of each image. The sequence is first processed by the EDSR super-resolution module, which upsamples all channels by $\times 4$ to match the reference ALS resolution. The super-resolved images are then passed through the UTAE encoder-decoder, which compresses the full temporal sequence using a temporal attention mechanism and outputs a single high-resolution canopy height map ($1 \times 1 \times 4H \times 4W$). Training is performed end-to-end using a Smooth L1 loss against ALS reference data, with gradients propagating through both UTAE and EDSR.

resolved output \hat{e}^f :

$$\hat{e}^f = \text{EDSR}(e^f) \in \mathbb{R}^{(B \cdot T) \times C \times H' \times W'} \quad (1)$$

where $H' = 4H$ and $W' = 4W$. Finally, the output is reshaped to restore the original temporal structure, producing the tensor $\hat{e} \in \mathbb{R}^{B \times T \times C \times H' \times W'}$.

Regression Module (UTAE). Then, the super-resolved sequence is forwarded to the UTAE regression model. The spatial encoder processes each image, after which the temporal encoder applies an attention mechanism to collapse the temporal dimension. By utilizing the day of the year associated with each acquisition, represented via sinusoidal functions, the model computes an attention mask to weight pixels based on their date, reducing the sequence to a single representative feature map. Finally, the spatial decoder reconstructs the canopy height map \hat{h} :

$$\hat{h} = \text{UTAE}(\hat{e}) \in \mathbb{R}^{B \times 1 \times H' \times W'} \quad (2)$$

where each pixel value corresponds to the predicted canopy height.

2.4. Implementation and Training Strategy

2.4.1. Training Data Sampling

During training, a 1×1 km tile was randomly sampled from the Open-Canopy dataset. To construct the time series, we identified the triplets ($S2, S1_{asc}, S1_{dsc}$) temporally closest to the reference ALS acquisition of this zone. The date assigned to each triplet corresponded to

the Sentinel-2 acquisition date. Tiles containing fewer than 4 distinct triplets were discarded from the training set. For the remaining tiles, as the model requires a fixed sequence length of $T = 16$, we padded sequences with an insufficient number of triplets by randomly duplicating existing ones or selected the 16 closest ones if more are available. These images were subsequently cropped into 64×64 pixel patches to match the model's input dimensions. Corresponding ALS canopy height references were extracted at the same coordinates with a 2.5 m resolution, yielding 256×256 pixel reference images.

2.4.2. Network Initialization and Optimization

The EDSR module was initialized using weights pre-trained on RGB images from the original study (Lim et al., 2017). As the data used in our model had more channels (optical and radar), the input and output weights of the model were adapted by assigning the additional channels the average of the three RGB channel weights as initialization.

As it is an end-to-end architecture, both parts of the model (EDSR and UTAE) were trained together. The super-resolution module was therefore not frozen, but optimized simultaneously with the rest of the network. Hence, it is no longer used as an image super-resolution model as such, but rather as an optimized sampling module, directly trained for the task of predicting canopy height.

The batch size was set to 2, with each training

sample consisting of a sequence of 16 triplet images ($S2, S1_{asc}, S1_{dsc}$), with each triplet image containing 14 channels. The ADAM optimizer (Kingma and Ba, 2017) was used with a learning rate of 1×10^{-4} . The loss function employed was a Smooth L1 loss⁶. A ReduceLROnPlateau⁷ scheduler was employed to reduce the learning rate by a factor of 0.1 whenever the validation loss failed to improve by at least 0.05 for 5 consecutive epochs. Early stopping was implemented with a patience of 10 and a minimum delta of 0.05 on the validation loss function. Training was performed on the Jean Zay supercomputer, using a node equipped with four NVIDIA Tesla V100 SXM2 32 GB GPUs and 40 Intel Cascade Lake 6248 CPUs.

2.4.3. Inference Protocol

During inference, for calculating metrics, predictions were made on patches of the same size as those used during training, i.e., 64×64 pixels. Inference was performed on the entire Open-Canopy test set by dividing these tiles into a grid of patches matching the model’s input size. To limit edge effects, each 256×256 pixel inference patch was cropped by 21 pixels on each side, and an additional margin of 20 pixels was retained to create an overlap zone between adjacent patches. In these overlapping areas, predictions were averaged, which smoothed the transition between patches and produced a more homogeneous final map.

2.5. Experimental Design

2.5.1. Ablation Study Setup

To evaluate the impact of different architectural components and identify the optimal configuration, we conducted an ablation study. The baseline architecture, denoted as SERA-H (EDSR-UTAE (16img)), combined the EDSR super-resolution module with the UTAE regression model using a sequence of 16 input images.

To assess the contribution of the super-resolution module, we trained a variant replacing EDSR with a standard $\times 4$ bilinear interpolation upsampling, denoted as BI-UTAE (16img). To analyze the influence of temporal modeling, two additional models employing a U-Net architecture instead of UTAE were evaluated. These models processed single composite images rather than time series and were designated as BI-UNet (bilinear interpolation upsampling) and EDSR-UNet (EDSR upsampling). These composites were generated using the

temporal mean for Sentinel-1 and the temporal median for Sentinel-2. Finally, to determine the sensitivity to the sequence length, we trained two variants of SERA-H with reduced temporal inputs: eight images (EDSR-UTAE (08img)) and four images (EDSR-UTAE (04img)). To reduce computational overhead during this comparative analysis, all models in the ablation study were trained on smaller input patches of 32×32 pixels.

2.5.2. Comparison with State-of-the-Art Methods

To evaluate the performance of SERA-H, we established a benchmarking protocol against five recent state-of-the-art (SOTA) methods: Fogel et al. (2025), Tolan et al. (2024), Liu et al. (2023), Schwartz et al. (2025), and Pauls et al. (2025). In the remainder of this paper, these models are referred to as Fogel, Tolan, Liu, Schwartz, and Pauls, respectively. These baselines differ in their supervision strategies and input data resolutions. On one hand, Schwartz and Pauls trained models using GEDI data on Sentinel-1 and Sentinel-2 imagery, producing height maps at a 10 m resolution. While Schwartz used standard temporal composites, Pauls exploited Sentinel-2 time series, using composites only for Sentinel-1. On the other hand, approaches based on commercial very high-resolution imagery all used data derived from ALS as a supervision reference: Tolan used 1 m Maxar imagery, Liu used 3 m PlanetScope imagery, and Fogel employed 1.5 m SPOT-6/7 images. Regarding the latter, it is worth noting that while SPOT imagery is generally commercial, the specific dataset used by Fogel is available free of charge for France through the Data Terra - DINAMIS⁸ institutional program.

Regarding temporal alignment, these baseline maps display varying degrees of consistency with our 2021–2023 validation dataset. Fogel and Schwartz were fully aligned with the validation period (2021–2023), while Pauls covered the years 2021 and 2022. Conversely, the global maps based on commercial imagery relied on slightly older acquisitions: Liu provided a map for the fixed year 2019, and Tolan aggregated imagery primarily between 2018 and 2020. For these latter models, we used the product temporally closest to our reference dates, acknowledging that minor discrepancies due to forest dynamics (e.g., growth or harvest) might theoretically affect the comparison.

To ensure a consistent quantitative evaluation at our reference resolution of 2.5 m, a standardization procedure was applied to all baseline predictions. Maps with a native resolution lower than the target (10 m and 3 m)

⁶<https://docs.pytorch.org/docs/stable/generated/torch.nn.SmoothL1Loss.html>

⁷https://docs.pytorch.org/docs/stable/generated/torch.optim.lr_scheduler.ReduceLROnPlateau.html

⁸<https://openspot-dinamis.data-terra.org/>

were upsampled using bilinear interpolation, whereas maps with a finer native resolution (1.5 m and 1 m) were downsampled using max pooling to preserve the top canopy height information.

2.5.3. Evaluation Metrics

The performance of the canopy height prediction model was evaluated using the Mean Absolute Error (MAE), Root Mean Squared Error (RMSE), Normalized Mean Absolute Error (nMAE), and Tree Cover IoU. All metrics, with the exception of Tree Cover IoU, were calculated only on pixels belonging to the vegetation mask described in Section 2.2.

Normalized Mean Absolute Error (nMAE). To assess the relative accuracy of the predictions, we computed the Normalized Mean Absolute Error (nMAE), defined as:

$$\text{nMAE} = \frac{1}{N} \sum_{i=1}^N \frac{|h_i - \hat{h}_i|}{h_i + 1} \quad (3)$$

where N is the total number of valid pixels, and h_i and \hat{h}_i denote the ALS reference and the predicted canopy height for pixel i , respectively. A regularization term of 1 m was added to the denominator to ensure numerical stability for low vegetation height. In addition to the vegetation mask, the nMAE was computed exclusively on pixels where the reference height exceeds 2 m, preventing the overestimation of errors in non-canopy areas.

Tree Cover IoU. To evaluate the accuracy of forest canopy detection and the sharpness of predictions, we implemented the Tree Cover IoU metric. To do this, we

generated two binary masks by applying a threshold of 2 m to the model predictions and reference data, above which we consider it to be the location of a tree. We then calculated the Intersection over Union (IoU) of these two “tree cover” masks, which gave us the final formula:

$$\text{Tree Cover IoU} = \text{IoU}(M_h, M_{\hat{h}}) = \frac{|M_h \cap M_{\hat{h}}|}{|M_h \cup M_{\hat{h}}|} \quad (4)$$

where $M_h = \{i \mid h_i \geq 2\}$ and $M_{\hat{h}} = \{i \mid \hat{h}_i \geq 2\}$ represent the binary vegetation masks for the reference and the model output, respectively. Although this indicator is only a derivative of the height threshold and does not provide an exact measurement of the canopy, it nevertheless allowed us to assess the extent to which the model correctly predicts the location of height areas.

3. Results

3.1. Ablation Study: Impact of Super-Resolution and Temporal Depth

Among all tested configurations, SERA-H (EDSR-UTAE with 16 images) achieved the best performances, with the best scores across all metrics in the test dataset (Table 1).

These results demonstrate that the super-resolution module substantially improves prediction quality compared to standard bilinear interpolation (BI). This trend is first observed on architectures based on composite mosaics: the EDSR-UNet model outperformed BI-UNet, reducing the Mean Absolute Error (MAE) by 0.30 m (from 3.39 m to 3.09 m) and the Root Mean Square Error (RMSE) by 0.34 m. This performance

Table 1: Ablation study. Evaluation of the impact of super-resolution (e.g., EDSR compared to Bilinear Interpolation, BI), the use of time series (e.g., UTAE compared to U-Net), and the sequence length (4, 8, or 16 triplet images) on canopy height prediction performance in the test area of the dataset. Note that to limit computational overhead, all models presented here were trained on reduced input patches of 32×32 pixels. *Params* denotes the total number of trainable parameters in millions. Best results are highlighted in **bold**.

Model Configuration	Params (M)	MAE (m)	RMSE (m)	nMAE (%)	Tree Cover IoU (%)
BI-UNet (mosaic)	31.0	3.39	4.90	27.55	83.57
BI-UTAE (16img)	1.1	3.35	4.84	26.78	83.91
EDSR-UNet (mosaic)	74.1	3.09	4.56	25.48	84.33
EDSR-UTAE (4img)	44.2	3.04	4.49	24.89	84.68
EDSR-UTAE (8img)	44.2	2.95	4.37	24.02	85.20
SERA-H (EDSR-UTAE (16img))	44.2	2.73	4.07	22.11	86.47

gain was even more pronounced for temporal architectures: replacing bilinear interpolation with EDSR within the UTAE model resulted in a significant reduction in MAE of 0.62 m (from 3.35 m for BI-UTAE to 2.73 m for SERA-H). These results confirm that training a dedicated upsampling module makes it possible to reconstruct the fine details of the canopy with much greater accuracy than conventional interpolation methods.

The use of the temporal dimension proved to be an equally important factor. Comparison of different architectures in Table 1 showed that models with time series (UTAE) consistently outperformed those based on static annual composites (U-Net). This efficiency was evident even in the configuration without super-resolution: the BI-UTAE model performed better than BI-UNet (MAE of 3.35 m vs. 3.39 m), while being notably lighter in terms of the number of parameters (1.1 million vs. 31 million). The gap widened further with the addition of super-resolution: the SERA-H temporal model improved the MAE by 0.36 m compared to its static equivalent EDSR-UNet (2.73 m vs. 3.09 m). These results confirm that the use of time series is a more relevant and effective approach than the use of mosaics for canopy height mapping.

Finally, the ablation study revealed a direct positive

correlation between the length of the input time series and the accuracy of the model. Reducing the number of images led to a gradual deterioration in performance. Specifically, the MAE increased by 0.22 m when using 8 instead of 16 images (from 2.73 m to 2.95 m), and worsened by an additional 0.09 m when retaining only 4 images (3.04 m). This confirmed that the model benefited from dense temporal sampling to resolve ambiguities in canopy structure. Given that the average availability per area in our dataset was 13.51 triplet images, the configuration of 16 triplets already exceeded this average. We therefore considered that exploring a model requiring an even longer sequence (e.g., 32 triplets) was not relevant.

3.2. Comparison with State-of-the-Art (SOTA)

3.2.1. Qualitative Evaluation

Qualitative evaluation is essential to complement quantitative results and provide a visual understanding of canopy height predictions. Fig. 4 compares the predictions from SERA-H with the SOTA methods, showcasing the differences in predicted canopy structure across various forest types.

Comparison with models trained on GEDI height. We acknowledge that a direct comparison of our model with

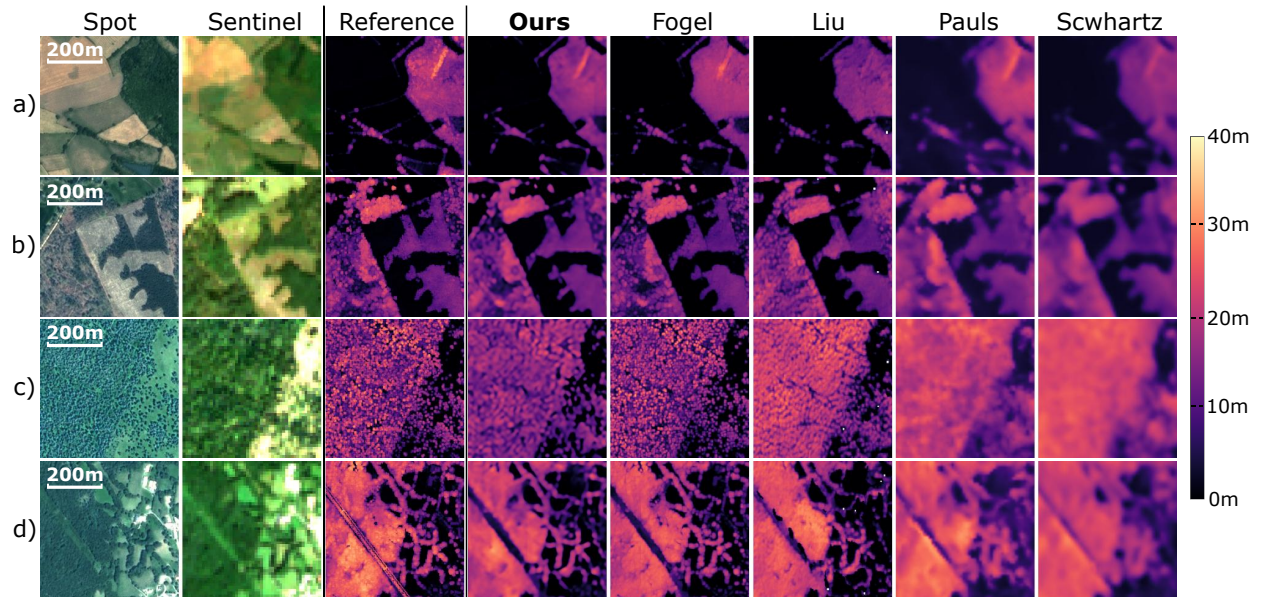


Figure 4: Qualitative comparison of predicted canopy height maps. Comparison of SERA-H with ALS reference data and four state-of-the-art canopy height maps (Fogel, Liu, Pauls, and Schwartz) over four selected study sites. The first two columns show the SPOT-6/7 and Sentinel-2 source images in RGB visualization. The third column displays the reference ALS-derived canopy height map at 2.5 m resolution. The following columns illustrate the canopy height estimates generated by each model. The study sites shown include: a) a chestnut grove in Aveyron (44.202°N, 2.262°E), b) a maritime pine forest in Dordogne (45.000°N, 0.309°E), c) a spruce forest in the Jura (46.344°N, 5.991°E), and d) a beech forest in the Alps (45.015°N, 5.793°E).

those of Pauls and Schwartz may not be entirely equitable. These models were trained using sparse GEDI data as a reference, resulting in inherent discrepancies when evaluated against dense ALS measurements. Furthermore, their outputs are naturally less sharp due to the lower resolution of their target grids (10 m). The purpose of this comparison is therefore not to directly match these models, but rather to demonstrate typical achievements using Sentinel data and to highlight the potential of our approach using the same input imagery.

Despite utilizing the same coarse-resolution Sentinel data, SERA-H generated predictions that surpassed the native resolution of the input. It produced clearer and more precise contours of forests and individual trees, allowing us to approach the scale of single-tree detection, which is significantly superior to other Sentinel-based products. This enhancement was largely driven by the use of ALS data as a reference, which provided a much higher frequency signal, enabling sharper and more accurate predictions. This confirms the utility of upsampling Sentinel images via a dedicated super-resolution method to align with the fine granularity of ALS data.

Comparison with models trained on ALS products. Liu trained their model on a much broader dataset covering all of Europe; consequently, their model is not specifically tailored to the French forest types targeted in our test dataset. Despite this, Liu’s model relies on commercial PlanetScope imagery, which has a resolution more than three times finer (3 m) than that of Sentinel. However, even against this higher-resolution input, SERA-H produced sharper, more precise predictions with clearer delineation of forest boundaries and individual trees.

The comparison with Fogel is the most relevant, as

it is based on the same training dataset (Open-Canopy) and the same ALS-based canopy height references. Although Fogel employed SPOT-6/7 imagery, which offers a spatial resolution nearly seven times higher (1.5 m) than our Sentinel inputs, SERA-H achieved a comparable prediction performance. While this resolution gap logically grants Fogel’s maps a finer level of textural detail, the ability of SERA-H to approach these performance metrics demonstrates the effectiveness of our super-resolution approach in bridging the gap between open-access and commercial imagery.

3.2.2. Quantitative Evaluation

In this section, we present the quantitative evaluation of SERA-H alongside other state-of-the-art models. Table 2 summarizes the performance metrics (detailed in Section 2.5.3) on the test dataset. To provide a more detailed analysis of the prediction errors, Fig. 5 illustrates the distribution of residuals across height bins, while Fig. 6 displays density scatterplots against the ALS reference data.

Comparison with models trained on GEDI height. As noted in Section 3.2.1, comparing our results with Pauls and Schwartz should be done with some caution, given their 10 m native resolution and reliance on GEDI reference. Metric discrepancies are therefore to be expected due to these differences in resolution and reference. However, as the height maps derived from ALS constitute the most reliable local estimate of canopy height at a very high resolution, it remains relevant to evaluate all models against this reference. Furthermore, this comparison allows us to identify the methodological benefit of SERA-H, revealing the accuracy improvement over existing methods that utilize Sentinel imagery

Table 2: Quantitative comparison between SERA-H and state-of-the-art methods. Our model is compared with Fogel, Liu, Tolan, Pauls and Schwartz, evaluated at a standardized resolution of 2.5 m. To match this resolution, finer maps were downsampled using maxpooling, while coarser maps were upsampled via bilinear interpolation. Input and reference images used for training each model are also specified in the columns 2 and 3, with their respective native resolutions provided in parentheses. Best results are highlighted in **bold**.

Model	Input Images	Reference Images	MAE (m)	RMSE (m)	nMAE (%)	Tree Cover IoU (%)
Pauls	S1-S2 (10m)	GEDI (10m)	5.13	7.24	42.06	45.58
Schwartz	S1-S2 (10m)	GEDI (10m)	4.47	6.17	45.96	35.12
Tolan	Maxar (1m)	ALS (1m)	5.49	7.52	41.74	70.15
Liu	Planet (3m)	ALS (3m)	4.40	6.20	37.44	78.42
Fogel	SPOT-6/7 (1.5m)	ALS (1.5m)	2.37	3.65	18.88	88.15
SERA-H	S1-S2 (10m)	ALS (2.5m)	2.60	3.86	20.40	87.25

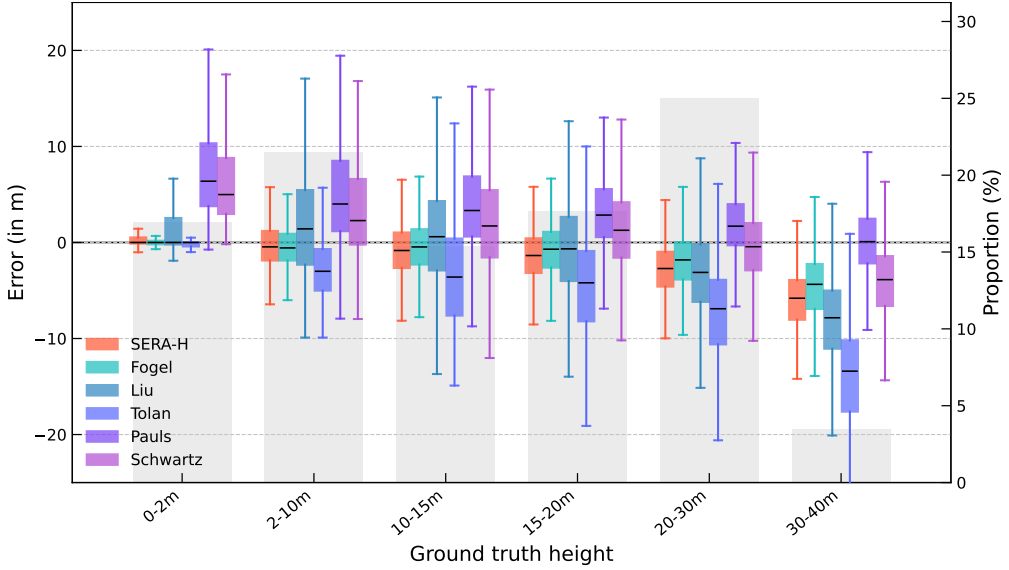


Figure 5: Distribution of prediction error across reference canopy height bins. The plot displays the error deviation (prediction – reference) for six models: SERA-H, Fogel, Liu, Tolan, Pauls, and Schwartz (primary y-axis, left). The shaded grey bars in the background represent the relative proportion of samples in each height class (secondary y-axis, right).

as input.

The results reported in Table 2 are consistent with the improved spatial detail observed in the maps (Section 3.2.1). SERA-H showed significantly lower errors than the Sentinel- and GEDI-based references: we obtained an MAE of 2.60 m, compared to 4.47 m for Schwartz and 5.13 m for Pauls. The relative error (nMAE) was also reduced by half (20.40% compared to over 42% for Pauls). Furthermore, with a Tree Cover IoU of 87.25% compared to a range of 35-45% for the other models, SERA-H demonstrated a much greater ability to correctly delineate vegetation. Finally, we verified these trends by calculating the metrics at a resolution of 10 m (Appendix A), corresponding to the native resolution of Sentinel images and related products. Although performance differences were reduced with spatial aggregation, the hierarchy of results remained the same. For example, for MAE, SERA-H obtained 3.00 m, while Pauls obtained 3.36 m and Schwartz obtained 3.72 m, confirming the robustness of our model’s predictions.

Further intercomparison analysis (Fig. 5 and Fig. 6) confirmed the good performance of the SERA-H model results. It highlights that models based on the Sentinel/GEDI pair systematically showed significantly greater error dispersion, as illustrated by more diffuse scatter plots and wider interquartile ranges. In addition, a strong tendency toward overestimation could be observed across most of the spectrum (0-30 m), where the

median errors were above zero. While performance became broadly comparable for the 20-30 m height class and the model by Pauls showed a lower median bias for trees exceeding 30 m, SERA-H nevertheless confirmed its overall superiority over models derived from Sentinel images.

Comparison with models trained on ALS products. Quantitative analysis (Table 2) shows that SERA-H significantly outperforms the approaches of Tolan and Liu. Despite the theoretical advantage conferred by the use of very high-resolution commercial images (PlanetScope at 3 m resolution and Maxar at 1 m), these models yielded Mean Absolute Errors (MAE) of 4.40 m and 5.49 m, respectively, which were higher than the 2.60 m obtained by SERA-H. This hierarchy is visually confirmed by the scatter plots (Fig. 6): where the predictions of Liu and Tolan showed high dispersion and struggled to follow the 1:1 line (with R^2 values of 0.581 and 0.376), SERA-H showed strong linearity ($R^2 = 0.818$). While this discrepancy could be explained partly by domain shift, given that Tolan was trained in the United States and Liu across Europe, these results suggest that excessive geographical generalization can be detrimental to local accuracy.

The comparison with Fogel is particularly important, as it used exactly the same dataset and reference images (Open-Canopy) as compared to SERA-H. The fundamental difference lies in the input images: Fogel uses

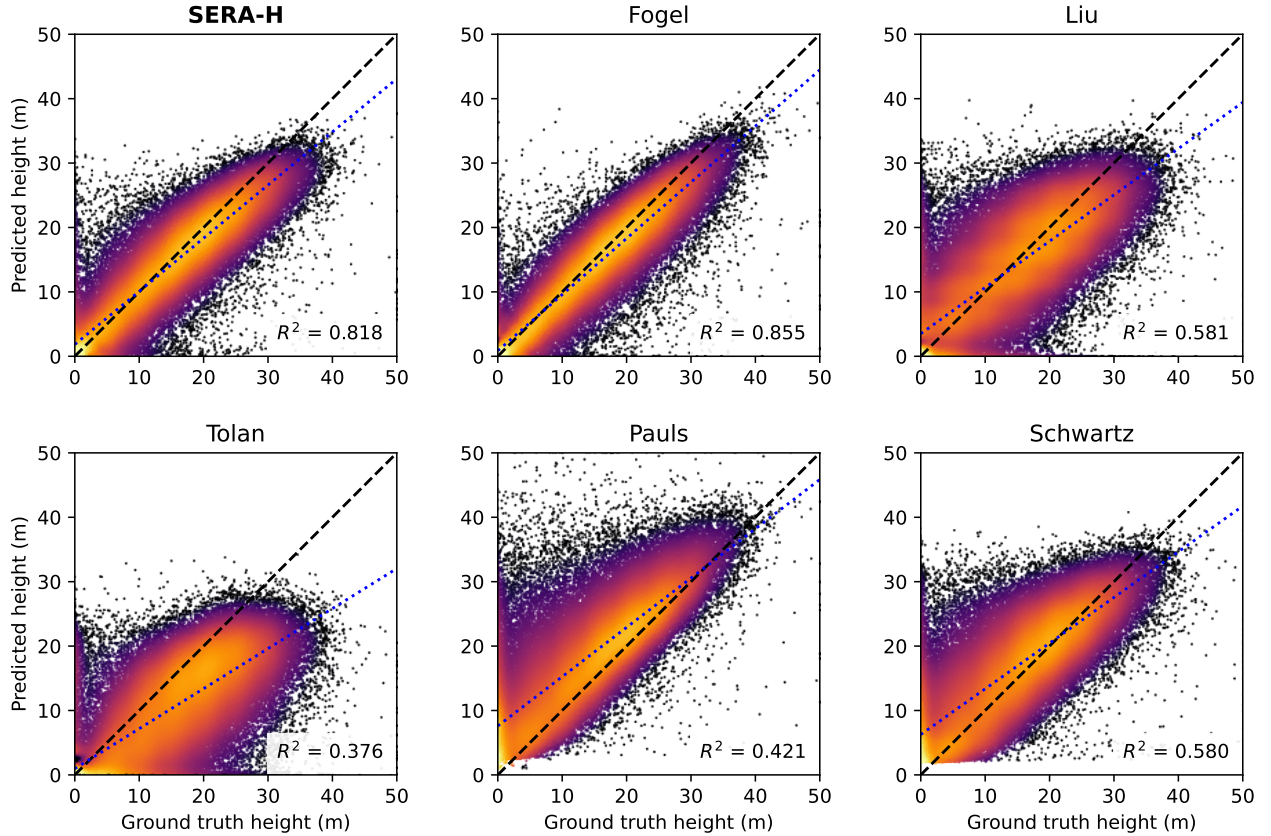


Figure 6: Scatter density plots comparing predicted canopy heights with ALS reference data. The panels display the performance of six models: SERA-H, Fogel, Liu, Tolan, Pauls, and Schwartz. The black dashed line indicates the perfect 1:1 fit, while the blue dotted line represents the linear regression. The coefficient of determination (R^2) is reported for each model. Note that for the Tolan model, a uniform noise in the range $[-0.5, 0.5]$ was applied to the original integer-valued predictions to enhance the visualization of point density; this adjustment does not affect the computed performance metrics. Brighter colors indicate a higher density of points.

SPOT-6/7 images (1.5 m) while SERA-H uses Sentinel-2 (10 m), which is nearly seven times lower in resolution. Despite this resolution disadvantage, SERA-H managed to match Fogel’s performance (MAE of 2.60 m vs. 2.37 m). This good performance of SERA-H could also be seen in the graphs: the scatter plots were almost identical and the boxplots (Fig. 5) revealed a similar error distribution, with medians close to zero and narrow interquartile ranges.

4. Discussion

Our results challenge the assumption that very high-resolution mapping of canopy height necessarily requires very high-resolution satellite imagery. By outperforming models based on PlanetScope 3 m imagery (Liu) and Maxar 1 m imagery (Tolan), SERA-H demonstrates that domain shift is more detrimental to local accuracy than the coarseness of the input pixels. Con-

versely, training on high-fidelity ALS reference data, while leveraging the abundant information provided by input time series, allows the model to reconstruct plausible fine structures, thereby decoupling the output resolution from the native resolution of the input image.

These results position SERA-H as a competitive alternative to approaches based on commercial higher-resolution imagery. Although Fogel obtained slightly sharper boundaries through the use of higher-resolution satellite images, SERA-H offers statistically comparable accuracy using only Sentinel-1 and Sentinel-2 data, which is freely available worldwide. Furthermore, while SPOT images are generally available on an annual basis, the Sentinel-1 and Sentinel-2 satellites offer a significantly higher revisit frequency. This temporal density allows estimates to be updated several times during the year, overcoming the constraint of static annual mapping and paving the way for possible intra-annual forest monitoring using freely available images.

Fig. 7 illustrates this potential with a few qualitative examples comparing height difference maps ($\Delta h = h_{t2} - h_{t1}$) obtained by ALS and by our model for forests in the Vosges region, France. For this comparison, the reference data was obtained from an initial IGN ALS campaign carried out in early 2020 (Ramirez Parra et al., 2024) and the 2022 LiDAR HD campaign⁹. By applying thresholds to identify major disturbance events, we observe that SERA-H seems to be able to identify and locate the main areas of deforestation (defined by a loss of at least -10 m). SERA-H could potentially serve as a monitoring or alert tool for clear-cutting, windfall, and other major losses, using fully accessible data.

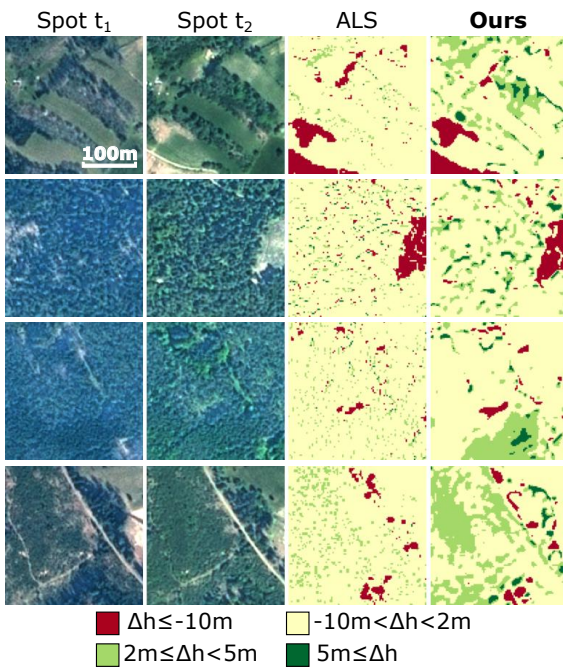


Figure 7: Qualitative analysis of forest dynamics in the Vosges region (Winter 2020-2022). The first two columns show SPOT-6/7 pan-sharpened images at 1.5 m resolution acquired on two separate dates ($t_1 = 2020$ and $t_2 = 2022$). The following columns illustrate the canopy height difference maps ($\Delta h = h_{t2} - h_{t1}$) derived respectively from the ALS reference and the SERA-H model predictions. Height variations are classified by thresholds: major losses (deforestation, ≤ -10 m) appear in red, stable or low variation areas (-10 to 2 m) in yellow, moderate growth (2 to 5 m) in light green, and strong growth (> 5 m) in dark green. All images are presented at the same scale.

However, analysis of these examples reveals a significant limitation concerning the detection of forest growth. The model struggles to accurately reproduce areas of moderate growth (2 to 5 m) or strong growth

(> 5 m) visible in the reference data. This result is consistent with the performance metrics: the natural growth of a temperate forest over a short period is often less than the model's Mean Absolute Error (MAE of 2.60 m). As a result, the growth signal tends to be concealed by prediction noise (model uncertainty). Thus, while SERA-H shows real potential for detecting spatially detailed forest disturbances, its use for quantifying fine-scale forest growth will require further development, particularly with regard to the temporal stabilization of predictions.

5. Conclusion and Limitations

In this paper, we introduced SERA-H, a new end-to-end model combining super-resolution and spatio-temporal learning to generate very high-resolution (2.5 m) canopy height maps from coarser (10 m) Sentinel-1 and Sentinel-2 imagery. Our methodology was validated through a comprehensive ablation study, which confirmed the critical role of the super-resolution module (EDSR) and the temporal attention mechanism (UTAE) in reconstructing fine canopy details that standard interpolation methods fail to capture. Furthermore, we benchmarked SERA-H against five recent state-of-the-art methods, ranging from Sentinel-based models trained on GEDI (Schwartz et al., 2025; Pauls et al., 2025) to approaches leveraging commercial very high-resolution imagery supervised by ALS data (Fogel et al., 2025; Tolan et al., 2024; Liu et al., 2023). The results demonstrate that, by leveraging the temporal density of open-access data, SERA-H not only outperforms other Sentinel-based models but also achieves accuracy comparable to, and in some cases superior to, models relying on costly commercial imagery. This effectively decouples prediction accuracy from input resolution, positioning SERA-H as a potential precise and cost-effective tool for forest management and biodiversity monitoring.

Despite these significant advances, the method is subject to intrinsic physical and methodological limitations. While SERA-H significantly refines the predicted canopy structure, it remains constrained by the spectral information available in 10 m input pixels; consequently, it cannot fully reconstruct small isolated trees or fine details that are spectrally indistinguishable at this resolution, whereas native very high-resolution imagery might still capture these features. Additionally, the model's performance is currently linked to the availability of high-density ALS data for supervision. Future work should therefore focus on evaluating the model's generalization capabilities in data-scarce regions, such as tropical or boreal biomes. To mitigate the dependence on dense LiDAR campaigns, exploring transfer learning

⁹<https://geoservices.ign.fr/lidarhd>

or weakly supervised techniques constitutes a promising direction for extending this approach to other areas.

Acknowledgements

We are grateful to Jean-Pierre Renaud from the Office National des Forêts (ONF) for providing the 2020 Vosges ALS dataset. This work was supported by the One Forest Vision Initiative (OFVi) and the AI4Forest project (ANR-22-FAI1-0002). We also acknowledge support from the Danish National Research Foundation through the Center for Remote Sensing and Deep Learning of Global Tree Resources (TreeSense, DNRF192). This work was performed using HPC resources from GENCI-IDRIS (Grants 2025-AD010114718R1 and 2026-AD010114718R2).

Data and Code Availability

The Open-Canopy dataset used in this study is available on Hugging Face at <https://huggingface.co/datasets/A14Forest/Open-Canopy>.

Declaration of Generative AI in the Writing Process

During the preparation of this work, the authors used Gemini and Chat-GPT to assist in writing code and improving the manuscript’s language and readability. After using this tool, the authors reviewed and edited the content as needed and take full responsibility for the content of the published article.

Appendix A. Evaluation at Standardized 10m Resolution

While models such as Liu, Tolan, and Fogel benefit from high-resolution input imagery, Sentinel-based approaches (e.g., Pauls and Schwartz) natively produce canopy height maps at a coarser resolution (10 m) than the 2.5 m target. Evaluating these models at this finer scale requires upsampling them using bilinear interpolation, which inherently introduces artifacts and may unfairly disadvantage them. To ensure a fair comparison between models operating at different native resolutions, we conducted an additional evaluation standardized at 10 m. For this purpose, we resampled all maps with a finer resolution to a 10 m grid using a *maximum pooling* operation.

The quantitative results presented in Table 3 confirm that Sentinel-2-based methods, such as Pauls and Schwartz, exhibit improved performance when evaluated at their native resolution of 10 m compared to finer scales. By avoiding upsampling artifacts, their Mean Absolute Errors drop to 3.72 m and 3.36 m, respectively.

Appendix B. Impact of Temporal Density on Model Performance

However, despite this more favorable evaluation setting for standard Sentinel-2 baselines, SERA-H maintains a significant performance lead across the dataset, achieving an MAE of 3.00 m. This superiority is particularly evident in the spatial accuracy of the predictions, as reflected by the Tree Cover Intersection over Union (IoU). While Pauls and Schwartz achieve IoU scores of approximately 55%, suggesting difficulties in precisely delineating canopy boundaries, SERA-H reaches a Tree

Model	Input images	Reference images	MAE (m)	RMSE (m)	nMAE (%)	Tree cover IoU (%)
Pauls 2025	S1-S2 (10m)	GEDI (10m)	3.72	4.90	23.19	55.71
Schwartz 2025	S1-S2 (10m)	GEDI (10m)	3.36	4.95	22.82	55.12
Tolan 2024	Maxar (1m)	ALS (1m)	6.31	8.24	39.38	71.37
Liu 2023	Planet (3m)	ALS (3m)	4.09	5.66	28.79	81.43
Fogel 2024	Spot 6-7 (1.5m)	ALS (1.5m)	2.44	3.62	15.81	89.95
SERA-H	S1-S2 (10m)	ALS (2.5m)	3.00	4.11	18.65	89.35

Table 3: Quantitative comparison between SERA-H (our model) and state-of-the-art methods (Fogel, Liu, Tolan, Pauls and Schwartz) evaluated at a standardized resolution of 10 m. All canopy height maps with finer native resolution were downsampled to 10 m using maximum pooling before metric calculation. Input and reference data sources are specified for each model in the column 2 and 3, with their respective native resolutions provided in parentheses.

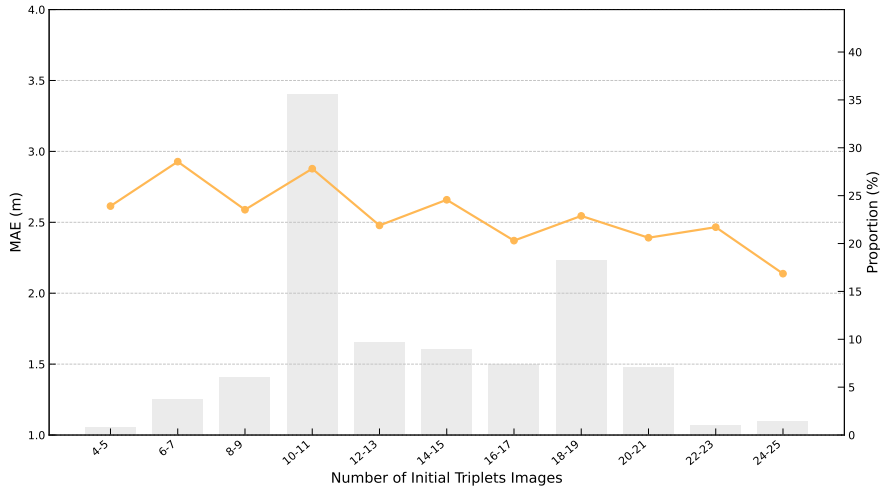


Figure A.8: Evolution of the Mean Absolute Error (MAE) of SERA-H as a function of the number of initial image triplets (orange curve, left axis). The grey bars represent the proportion of samples in the test dataset for each bin (right axis). The number of triplets refers to the number of unique acquisitions available before the duplication or truncation process used to reach the fixed input sequence length of 16 required by SERA-H

Cover IoU of 89.35%. This result highlights our model’s ability to correctly localize vegetation, rivalling the performance of Fogel’s high-resolution method (89.95%) and demonstrating that SERA-H successfully reconstructs fine spatial details even from coarser input data.

To assess the robustness of SERA-H regarding data availability, we analyzed the Mean Absolute Error (MAE) as a function of the number of available image triplets ($S2, S1_{asc}, S1_{dsc}$) before the duplication or truncation step.

As illustrated in Fig. A.8, the model performance improves slightly as the number of available triplets increases, which is expected since the model is provided with more temporal information. However, the MAE remains remarkably stable even for sequences with a low number of initial images. This stability demonstrates the model’s capacity to effectively reconstruct canopy height even when temporal density is sparse.

References

Alexander, C., Korstjens, A.H., Hill, R.A., 2018. Influence of micro-topography and crown characteristics on tree height estimations in tropical forests based on LiDAR canopy height models. International Journal of Applied Earth Observation and Geoinformation 65, 105–113. URL: <https://www.sciencedirect.com/science/article/pii/S0303243417302283>, doi:10.1016/j.jag.2017.10.009.

Ayala, C., Aranda, C., Galar, M., 2022. Pushing the Limits of Sentinel-2 for Building Footprint Extrac-

tion, in: IGARSS 2022 - 2022 IEEE International Geoscience and Remote Sensing Symposium, pp. 322–325. URL: <https://ieeexplore.ieee.org/document/9883103/?arnumber=9883103>, doi:10.1109/IGARSS46834.2022.9883103. iSSN: 2153-7003.

Belouze, G., Purnell, D., Rechatin, H., 2025. GeeFetch. URL: <https://github.com/gbelouze/geefetch>. original-date: 2024-06-12T18:12:07Z.

Bossy, T., Ciais, P., Renaudineau, S., Wan, L., Ygorra, B., Adam, E., Barbier, N., Bauters, M., Delbart, N., Frappart, F., Gara, T.W., Hamunyela, E., Ifo, S.A., Jaffrain, G., Maisongrande, P., Mugabowindekwe, M., Mugiraneza, T., Normandin, C., Obame, C.V., Peaucelle, M., Pinet, C., Ploton, P., Sagang, L.B., Schwartz, M., Sollier, V., Sonké, B., Tresson, P., De Truchis, A., Vo Quang, A., Wigneron, J.P., 2025. State of the art in remote sensing monitoring of carbon dynamics in African tropical forests. Frontiers in Remote Sensing 6. URL: [https://www.frontiersin.org/journals/remote-sensing/articles/10.3389/frsen.2025.1532280](https://www.frontiersin.org/journals/remote-sensing/articles/10.3389/frsen.2025.1532280/full). publisher: Frontiers.

Chen, S., Ogawa, Y., Zhao, C., Sekimoto, Y., 2023. Large-scale individual building extraction from open-source satellite imagery via super-resolution-based instance segmentation approach. ISPRS Journal of Photogrammetry and Remote Sensing 195, 129–152. URL: <https://www.sciencedirect.com/sc>

[ience/article/pii/S0924271622002933](https://doi.org/10.1016/j.isprsjprs.2022.11.006), doi:10.1016/j.isprsjprs.2022.11.006.

Fischer, F.J., Morgan, B., Jackson, T., Chave, J., Coomes, D., Cushman, K.C., Dalagnol, R., Dalponte, M., Duncanson, L., Saatchi, S., Seidl, R., Stereńczak, K., Laurin, G.V., Adu-Bredou, S., Aguirre-Gutiérrez, J., Antonielli, B., Armston, J.D., Assis, M.L.d., Barbier, N., Burt, A., César, R.G., Cervenka, J., Coops, N., Cullen, L., Dalling, J.W., Davies, A., Demol, M., Ebenbeck, J., Fassnacht, F., Fatoynibo, L., García, M., Gasparri, N.I., Gobakken, T., Goodbody, T.R.H., Görgens, E.B., Gorum, T., Gosper, C., Guan, H., Heiskanen, J., Heurich, M., Hobi, M., Höfle, B., Hooijer, A., Huth, A., Kedrov, A., Kellner, J.R., Koenig, S., Král, K., Krassovski, M., Kuechly, H., Krůček, M., Htoo, K.K., Labrière, N., Lai, D., Larson, J., Laudon, H., Lemke, D., Lenoir, J., Malhi, Y., Malik, O.A., Martin, M., McNicol, I., Milenkovic, M., Minor, D., Mitchard, E., Moudrý, V., Muller-Landau, H.C., Næsset, E., Nathalang, A., Ometto, J.P., Onishi, M., Onoda, Y., Pellikka, P., Persson, H., Ferreira, M.P., Ploton, P., Prober, S.M., Rahman, F., Rana, P., Réjou-Méchain, M., Schäfer, J., Senf, C., Shapiro, A., Schepaschenko, D., Shen, G., Silman, M., Silva, T., Singh, J., Slik, F., Stillhard, J., Subash, A., Takeshige, R., Tao, S., Tenorio, E., Tokola, T., Tompalski, P., Tripathi, N., Valbuena, R., Valentini, R., Vernimmen, R., Vincent, G., Wallerman, J., Jaafar, W.S.W.M., Wang, Y., Weiser, H., White, J., Winiwarter, L., Wulder, M., Yuan, Z., Zdunic, K., Zeng, Y., Zhang, H., Zhang, J., Zhang, Z., Jucker, T., 2025. The Global Canopy Atlas: analysis-ready maps of 3D structure for the world's woody ecosystems. URL: <https://www.biorxiv.org/content/10.1101/2025.08.31.673375v2>, doi:10.1101/2025.08.31.673375. iSSN: 2692-8205 Pages: 2025.08.31.673375 Section: New Results.

Fogel, F., Perron, Y., Besic, N., Saint-André, L., Pellissier-Tanon, A., Schwartz, M., Boudras, T., Fayad, I., d'Aspremont, A., Landrieu, L., Ciais, P., 2025. Open-Canopy: Towards Very High Resolution Forest Monitoring, in: 2025 IEEE/CVF Conference on Computer Vision and Pattern Recognition (CVPR), pp. 1395–1406. URL: <https://ieeexplore.ieee.org/document/11095116>, doi:10.1109/CVPR52734.2025.00138. iSSN: 2575-7075.

Garnot, V.S.F., Landrieu, L., 2022. Panoptic Segmentation of Satellite Image Time Series with Convolutional Temporal Attention Networks. URL: <http://arxiv.org/abs/2107.07933>, doi:10.48550/arXiv.2107.07933 [cs].

//arxiv.org/abs/2107.07933, doi:10.48550/arXiv.2107.07933. arXiv:2107.07933 [cs].

Goetz, S.J., Steinberg, D., Betts, M.G., Holmes, R.T., Doran, P.J., Dubayah, R., Hofton, M., 2010. Lidar remote sensing variables predict breeding habitat of a Neotropical migrant bird. *Ecology* 91, 1569–1576. doi:10.1890/09-1670.1.

Guo, M., Zhang, Z., Liu, H., Huang, Y., 2022. ND-SRGAN: A Novel Dense Generative Adversarial Network for Real Aerial Imagery Super-Resolution Reconstruction. *Remote Sensing* 14, 1574. URL: <https://www.mdpi.com/2072-4292/14/7/1574>, doi:10.3390/rs14071574. publisher: Multidisciplinary Digital Publishing Institute.

Jiang, K., Wang, Z., Yi, P., Wang, G., Lu, T., Jiang, J., 2019. Edge-Enhanced GAN for Remote Sensing Image Superresolution. *IEEE Transactions on Geoscience and Remote Sensing* 57, 5799–5812. URL: <https://ieeexplore.ieee.org/document/8677274>, doi:10.1109/TGRS.2019.2902431.

Karwowska, K., Wierzbicki, D., 2022. Using Super-Resolution Algorithms for Small Satellite Imagery: A Systematic Review. *IEEE Journal of Selected Topics in Applied Earth Observations and Remote Sensing* 15, 3292–3312. URL: <https://ieeexplore.ieee.org/document/9757881/>, doi:10.1109/JSTARS.2022.3167646. 12 citations (Crossref) [2024-06-20].

Kingma, D.P., Ba, J., 2017. Adam: A Method for Stochastic Optimization. URL: <http://arxiv.org/abs/1412.6980>, doi:10.48550/arXiv.1412.6980. arXiv:1412.6980 [cs].

Lang, N., Jetz, W., Schindler, K., Wegner, J.D., 2023. A high-resolution canopy height model of the Earth. *Nature Ecology & Evolution* 7, 1778–1789. URL: <https://www.nature.com/articles/s41559-023-02206-6>, doi:10.1038/s41559-023-02206-6. publisher: Nature Publishing Group.

Ledig, C., Theis, L., Huszar, F., Caballero, J., Cunningham, A., Acosta, A., Aitken, A., Tejani, A., Totz, J., Wang, Z., Shi, W., 2016. Photo-Realistic Single Image Super-Resolution Using a Generative Adversarial Network. URL: <https://arxiv.org/abs/1609.04802v5>.

Lefsky, M.A., Cohen, W.B., Harding, D.J., Parker, G.G., Acker, S.A., Gower, S.T., 2002. Lidar remote sensing of above-ground biomass in three biomes. *Global*

Ecology and Biogeography 11, 393–399. URL: <https://onlinelibrary.wiley.com/doi/abs/10.1046/j.1466-822x.2002.00303.x>, doi:10.1046/j.1466-822x.2002.00303.x. eprint: <https://onlinelibrary.wiley.com/doi/pdf/10.1046/j.1466-822x.2002.00303.x>.

Lefsky, M.A., Harding, D.J., Keller, M., Cohen, W.B., Carabajal, C.C., Del Bom Espírito-Santo, F., Hunter, M.O., de Oliveira Jr., R., 2005. Estimates of forest canopy height and aboveground biomass using ICESat. *Geophysical Research Letters* 32. URL: <https://agupubs.onlinelibrary.wiley.com/doi/abs/10.1029/2005GL023971>, doi:<https://doi.org/10.1029/2005GL023971>.

Lim, B., Son, S., Kim, H., Nah, S., Lee, K.M., 2017. Enhanced Deep Residual Networks for Single Image Super-Resolution. URL: <http://arxiv.org/abs/1707.02921>, doi:10.48550/arXiv.1707.02921. arXiv:1707.02921 [cs].

Liu, S., Brandt, M., Nord-Larsen, T., Chave, J., Reiner, F., Lang, N., Tong, X., Ciais, P., Igel, C., Li, S., Mugabowindekwe, M., Saatchi, S., Yue, Y., Chen, Z., Fensholt, R., 2023. The overlooked contribution of trees outside forests to tree cover and woody biomass across Europe. URL: <https://www.researchsquare.com/article/rs-2573442/v1>, doi:10.21203/rs.3.rs-2573442/v1. iSSN: 2693-5015.

Pauls, J., Zimmer, M., Turan, B., Saatchi, S., Ciais, P., Pokutta, S., Gieseke, F., 2025. Capturing Temporal Dynamics in Large-Scale Canopy Tree Height Estimation. URL: <https://arxiv.org/abs/2501.19328v1>.

Ramirez Parra, L.A., Renaud, J.P., Vega, C., 2024. How reliable are remote sensing maps calibrated over large areas? A matter of scale? URL: <https://arxiv.org/abs/2408.03953v1>.

Ren, P., Erichson, N.B., Subramanian, S., San, O., Lukic, Z., Mahoney, M.W., 2023. SuperBench: A Super-Resolution Benchmark Dataset for Scientific Machine Learning. URL: <http://arxiv.org/abs/2306.14070>, doi:10.48550/arXiv.2306.14070. arXiv:2306.14070 [physics].

Ronneberger, O., Fischer, P., Brox, T., 2015. U-Net: Convolutional Networks for Biomedical Image Segmentation. URL: <http://arxiv.org/abs/1505.04597>, doi:10.48550/arXiv.1505.04597. arXiv:1505.04597 [cs].

Schwartz, M., Ciais, P., De Truchis, A., Chave, J., Ottlé, C., Vega, C., Wigneron, J.P., Nicolas, M., Jouaber, S., Liu, S., Brandt, M., Fayad, I., 2023. FORMS: Forest Multiple Source height, wood volume, and biomass maps in France at 10 to 30 m resolution based on Sentinel-1, Sentinel-2, and Global Ecosystem Dynamics Investigation (GEDI) data with a deep learning approach. *Earth System Science Data* 15, 4927–4945. URL: <https://essd.copernicus.org/articles/15/4927/2023/>, doi:10.5194/essd-15-4927-2023. publisher: Copernicus GmbH.

Schwartz, M., Ciais, P., Sean, E., de Truchis, A., Vega, C., Besic, N., Fayad, I., Wigneron, J.P., Brood, S., Pelissier-Tanon, A., Pauls, J., Belouze, G., Xu, Y., 2025. Retrieving yearly forest growth from satellite data: A deep learning based approach. *Remote Sensing of Environment* 330, 114959. URL: <https://www.sciencedirect.com/science/article/pii/S0034425725003633>, doi:10.1016/j.rse.2025.114959.

Sirko, W., Brempong, E.A., Marcos, J.T.C., Annkah, A., Korme, A., Hassen, M.A., Sapkota, K., Shekel, T., Diack, A., Nevo, S., Hickey, J., Quinn, J., 2023. High-Resolution Building and Road Detection from Sentinel-2. URL: <https://arxiv.org/abs/2310.11622v3>.

Su, Y., Besic, N., Zhang, X., Xu, Y., Francini, S., D'Amico, G., Chirici, G., Schwartz, M., Fayad, I., Brood, S., Pellissier-tanon, A., Yu, K., Chen, H., Chen, S., d'Aspremont, A., Ciais, P., 2025a. A fused canopy height map of Italy (2004–2024) from spaceborne and airborne LiDAR, and Landsat via deep learning and Bayesian averaging. *Earth System Science Data Discussions*, 1–25 URL: <https://essd.copernicus.org/preprints/essd-2025-378/>, doi:10.5194/essd-2025-378. publisher: Copernicus GmbH.

Su, Y., Schwartz, M., Fayad, I., García, M., Zavala, M.A., Tijerín-Triviño, J., Astigarraga, J., Cruz-Alonso, V., Liu, S., Zhang, X., Chen, S., Ritter, F., Besic, N., d'Aspremont, A., Ciais, P., 2025b. Canopy height and biomass distribution across the forests of Iberian Peninsula. *Scientific Data* 12, 678. URL: <https://www.nature.com/articles/s41597-025-05021-9>, doi:10.1038/s41597-025-05021-9. publisher: Nature Publishing Group.

Tolan, J., Yang, H.I., Nosarzewski, B., Couairon, G., Vo, H.V., Brandt, J., Spore, J., Majumdar, S., Haziza, D., Vamaraju, J., Moutakanni, T., Bojanowski, P.,

Johns, T., White, B., Tiecke, T., Couprie, C., 2024. Very high resolution canopy height maps from RGB imagery using self-supervised vision transformer and convolutional decoder trained on aerial lidar. *Remote Sensing of Environment* 300, 113888. URL: <https://www.sciencedirect.com/science/article/pii/S003442572300439X>, doi:10.1016/j.rse.2023.113888.

Tomppo, E., 2008. Methods, in: Haakana, M., Katila, M., Peräsaari, J. (Eds.), *Multi-Source National Forest Inventory: Methods and Applications*. Springer Netherlands, Dordrecht, pp. 35–62. URL: https://doi.org/10.1007/978-1-4020-8713-4_3, doi:10.1007/978-1-4020-8713-4_3.

Zhang, L., Dong, R., Yuan, S., Li, W., Zheng, J., Fu, H., 2021. Making Low-Resolution Satellite Images Reborn: A Deep Learning Approach for Super-Resolution Building Extraction. *Remote Sensing* 13, 2872. URL: <https://www.mdpi.com/2072-4292/13/15/2872>, doi:10.3390/rs13152872. number: 15 Publisher: Multidisciplinary Digital Publishing Institute.